Letter

Mono-X signal and two component dark matter: New distinction criteria

Subhaditya Bhattacharya,[1,*] Purusottam Ghosh,[2,†] Jayita Lahiri,[3,‡] and Biswarup Mukhopadhyaya[4,§]

[1]*Department of Physics, Indian Institute of Technology Guwahati, Assam-781039, India*
[2]*School Of Physical Sciences, Indian Association for the Cultivation of Science, 2A and 2B, Raja S.C. Mullick Road, Kolkata 700032, India*
[3]*II. Institut für Theoretische Physik, Universität Hamburg, Luruper Chaussee 149, 22761 Hamburg, Germany*
[4]*Department of Physical Sciences, Indian Institute of Science Education and Research Kolkata, Mohanpur—741246, India*

(Received 1 February 2023; accepted 17 November 2023; published 14 December 2023)

The identification and isolation of two weakly interacting massive particles (WIMP) dark matter (DM) components at colliders is of wide interest on the one hand but extremely challenging on the other, especially when the dominant signal of both DM components is of the mono-X type ($X = \gamma, Z, H$). After emphasizing that an e^+e^- collider is more suitable for this goal, we first identify the theoretical principles that govern the occurrence of two peaks in missing energy ($\not{E}$) distribution, in a double-DM scenario. We then identify a variable that rather spectacularly elicits the double-peaking behavior, namely, the plot of bin-wise statistical significance ($S/\sqrt{B}$) against $\not{E}$. Using Gaussian fits of the histograms, we apply a set of criteria developed by us, to illustrate the above points numerically for suitable benchmarks.

DOI: 10.1103/PhysRevD.108.L111703

Given that the visible sector of the universe comprises of multiple particle components at various mass scales, having more than one weakly interacting massive particles (WIMP) as DM components is quite viable [1–6] and intriguing. Moreover, multicomponent DM frameworks provide some interesting dynamics and phenomenology like manifesting modified freeze-out, relaxing direct and indirect search bounds, addressing structure formation etc.

Multicomponent DM's should in general lead to missing energy ($\not{E}$) or missing transverse energy ($\not{E}_T$) at colliders. However, distinguishing two DM components in collider experiments is rather challenging in general, and is possible under certain circumstances only. The task is especially arduous if the major collider signal consists in mono-X plus $\not{E}$ (with $X = \gamma, Z, H$), primarily due to the very limited number of kinematic variables at our disposal, and partially due to the apparent insurmountability of Standard Model (SM) backgrounds. The present work is aimed at meeting such challenges.

*subhab@iitg.ac.in
†spspg2655@iacs.res.in
‡jayita.lahiri@desy.de
§biswarup@iiserkol.ac.in

Published by the American Physical Society under the terms of the Creative Commons Attribution 4.0 International license. Further distribution of this work must maintain attribution to the author(s) and the published article's title, journal citation, and DOI. Funded by SCOAP³.

e^+e^- colliders may be better suited for isolating two WIMP DM particles if they are kinematically accessible. This is mainly due to (a) the possibility of using $\not{E}$ as a variable, which depends on DM mass, (b) availability of missing longitudinal momentum as a source of extra information, (c) less SM background contamination, and (d) the advantage of initial beam polarization [7,8]. The rest of the discussion is therefore in the context of e^+e^- machines. We illustrate the criteria for double-DM signals being identifiable in e^+e^- colliders, using some phenomenologically selected benchmarks. In particular, we suggest a variable that rather spectacularly enables the distinction between the two DM components, namely, the bin-wise signal significance in the missing-energy distribution.

Challenge 1: Will there always be noticeable peaks/bumps? Mono-X signals are generic to any WIMP model, which result from direct production of a DM pair (when the DM is stabilized by a symmetry such as Z_2) typically in absence of an extended dark sector [9–14]. It has the simplest event topology, and at the same time leaves one with limited choice in analysing the final state kinematics. Bumps in $\not{E}$ distributions are driven by both kinematics and dynamics. Kinematics decide the minimum and maximum $\not{E}$ for a given event, which in turn depend on the center-of-mass (c.m.) energy and DM masses. Energy-momentum conservation plays an important role here. On the other hand, the shape of the $\not{E}$ distribution, both at the edges and in between, depends on the dynamics, namely, the Lagrangian, including possible sources of soft or collinear divergence.

TABLE I. Samples of DM-SM EFT operators involving isosinglet DM (χ) as scalar or fermion. $B_{\mu\nu}$ and $W_{\mu\nu}$ are electroweak field strength tensors, $L(\ell_R)$ are left (right)-handed SM lepton doublet (singlet), Φ is the SM Higgs doublet, D_μ is the gauge-covariant derivative, c is the Wilson coefficient and Λ is the cutoff scale of the EFT operators.

DM-type	Name	Operator
Scalar	O_1^s	$\frac{c}{\Lambda^2}(\bar{L}\Phi\ell_R)(\chi^2)$
Scalar	O_2^s	$\frac{c}{\Lambda^4}(\bar{L}D_\mu\Phi\ell_R)(\chi\partial_\mu\chi)$
Scalar	O_3^s	$\frac{c}{\Lambda^2}(B_{\mu\nu}B^{\mu\nu}+W_{\mu\nu}W^{\mu\nu})(\chi^2)$
Fermion	O_1^f	$\frac{c}{\Lambda^2}(\bar{L}\gamma^\mu L+\overline{\ell}_R\gamma^\mu\ell_R)(\bar{\chi}\gamma_\mu\chi)$
Fermion	O_2^f	$\frac{c}{\Lambda^3}(\bar{L}\Phi\ell_R)(\bar{\chi}\chi)$
Fermion	O_3^f	$\frac{c}{\Lambda^3}(B_{\mu\nu}B^{\mu\nu}+W_{\mu\nu}W^{\mu\nu})(\bar{\chi}\chi)$

In order to explore the features of two-component DM in a model-independent manner we take up an effective field theory (EFT) approach as it suffices to address the DM saturation as well as detectability. Table I shows a set of EFT operators involving a isosinglet DM (χ), stabilized by a Z_2 symmetry, interacting with SM particles which can lead to $e^+e^- \to \chi\chi X$ ($X = \gamma, Z, H$) [15–18]. This can happen via either $2 \to 3$ hard scattering, or through $2 \to 2$ DM pair production along with radiation of a γ, Z or H from one of the legs. The benchmarks on which we base our illustrative numerical predictions include dual-DM scenarios with both scalars, fermions and combinations of them. Note further that the operators listed here are merely indicative, and by no means constitute an exhaustive list. However, whether the bump-hunting approach works for a particular operator depends on the following principles:

(1) Angular momentum conservation: This is often related to the chiral structure of the interactions involved. There can be situations where a particular spatial configuration and the relative directionality of the particles is not allowed by the angular momentum conservation, given the helicity assignments demanded by the underlying interactions. In that case we see a drop in the differential distribution in $\frac{d\sigma}{d\not{E}}$ or zeroes at the edge(s) of the phase space, providing a peaking behavior.

(2) Rotational invariance in Minkowski space ($E^2 - |p|^2 = m^2$): The last integrand before arriving at the differential distribution such as $\frac{d\sigma}{d\not{E}}$, always contains a positive power of the of three-momentum of a final state particle. Therefore the final state particles being at rest automatically causes the differential distribution to vanish resulting a peaklike behavior, unless the drop is assuaged by a factor in the denominator, where the same three-momentum occurs.

(3) Collinear divergence: Arises when the radiated γ is collinear to the initial or final state particles and dominantly controls features of the distributions. A massive propagator which does not lead to collinear divergence, may still lead, instead of a drop, to a rise at an edge of the phase space due to a three momentum factor in the denominator. A soft photon corresponding to the maximum of $\not{E}$, accompanied by an infrared divergence, may also cause such a rise.

(4) Operator structure: The exact position of the maxima of the distributions are often dictated by the specific interaction in question.

(5) DM mass ($m_{\rm DM}$): The left-edge of the $\not{E}$ distribution, i.e., the minimum possible $\not{E}$ depends on $m_{\rm DM}$. Sizes of the peaks depend on the production cross-section, which in turn also depends on $m_{\rm DM}$ together with c and Λ.

Our study is centred around double bump hunting in $\not{E}$ distributions coming from two DM components. It is worth mentioning that, when two DM-components stem from the same operator having same spin, the higher mass DM having smaller production cross-section gets hidden beneath the tail of the larger peak, failing to produce a double-peak behavior, see the Supplemental Material [19] for example.

In Fig. 1 (top) we show an example of $\not{E}$ distributions in mono-γ signal, where double peak behavior is observed, when two DM particles from two different operators O_3^s and O_2^f are pair-produced in e^+e^- collision at $\sqrt{s} = 1$ TeV. The peaking behavior around the minimum of $\not{E}$ is obtained because (i) there is no collinear divergence at this kinematic point, and (ii) this region is not disfavored by angular momentum conservation, thanks to the chiral structure of the interaction responsible for this peak (O_3^s). O_3^s provides a photon mediated final state consisting of a photon and two scalar DM's. The resultant spin one state provides the minimum $\not{E}$ configuration when the photon emerges opposite to the two DM particles. The rise at the maximum of $\not{E}$, on the other hand, is because of collinear as well as infrared divergence, since the γ emitted is not only "soft" but also at a small angle with the initial $e^\pm$, something that in this case is not disfavored by the angular momentum conservation. This is clear from Fig. 1 (bottom), where we show the individual contributions from the two DM components (O_3^s in red and O_2^f in purple) to the $\not{E}$ signal distribution as shown by the blue line in top.

We note here that the double peaking behavior can also arise from a single DM component, when $m_{\rm DM}$ is very small compared to $\sqrt{s}$, since a collinear divergence can then occur even at the minimum of $\not{E}$ or when it interacts via different operators, as shown in the Supplemental Material [19]. On the other hand, the combined $\frac{d\sigma}{d\not{E}}$ distributions for two DM particles from two different operators can provide a single peak, when the individual distributions are identical and shows a collinear shoot-up at the maximum $\not{E}$ and a suppression

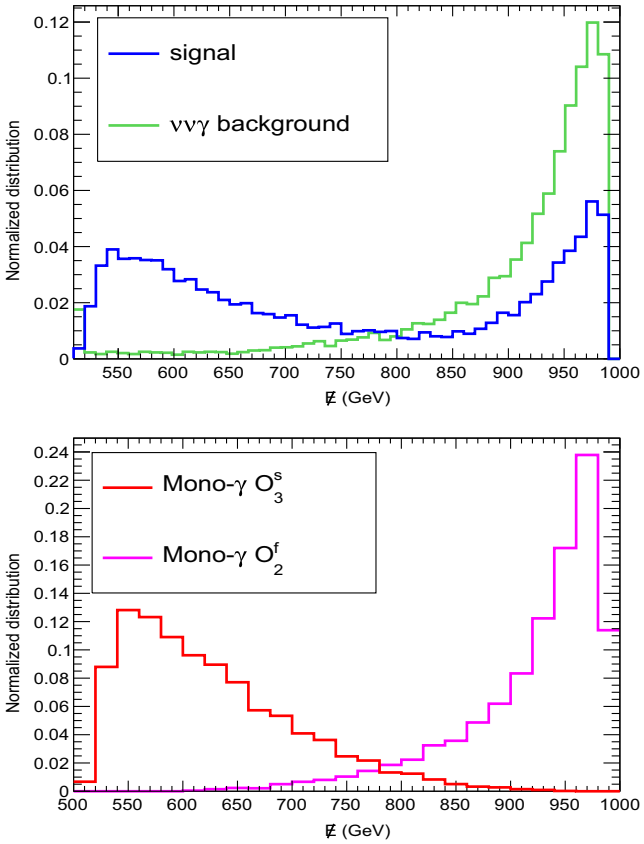


FIG. 1. Top: normalized $\not{E}$ distribution in the mono-γ final state for two DM components arising from O_3^s and O_2^f operators, for DM masses 100 GeV and 200 GeV respectively, together with $\nu\bar{\nu}\gamma$ background. Bottom: individual normalized distributions of $\not{E}$ in the mono-γ final state coming from the two DM candidates of masses 100 GeV (O_3^s) and 200 GeV (O_2^f). For both figures, we choose $\sqrt{s} = 1$ TeV, $\Lambda = 1.2$ TeV with $P_{e^+} = +30\%, P_{e^-} = +80\%$.

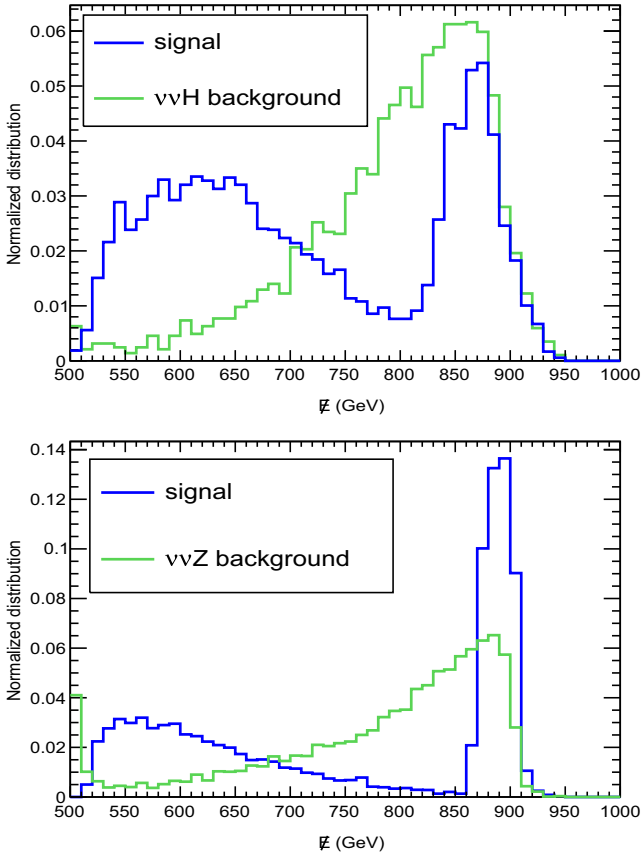


FIG. 2. Normalized $\not{E}$ distribution for (top) mono-H final state for two DM components from O_2^s and O_1^s, (bottom) mono-Z final state for two DM components arising from O_3^s and O_1^f, with masses 100 GeV and 400 GeV respectively. SM backgrounds are also shown. We choose $\sqrt{s} = 1$ TeV, $\Lambda = 1.2$ TeV and $P_{e^+} = +30\%, P_{e^-} = +80\%$.

at the minimum $\not{E}$ due to the structure of relevant operators. This is avoidable if one of the two mono-γ generating processes is driven by an effective interaction vertex as chosen above, as opposed to the case where the photon is emitted via bremsstrahlung.

Next, we take up the mono-H and mono-Z signals, illustrative predictions for which are shown in Fig. 2. O_2^s and O_1^s for mono-H (top panel), O_3^s and O_1^f are considered for mono-Z (bottom panel) with details of the parameters stated in the caption. We have reconstructed the mono-Z and mono-H events in the $\ell^+\ell^-(\ell = e, \mu)$ and $b\bar{b}$ channel, respectively, with the standard trigger and selection cuts. For both the plots in Fig. 2, the distribution is brought down to zero for maximum $\not{E}$. The reason behind this being the occurrence of $(E^2 - m^2)$ in the numerator of the penultimate integrand in cross-section calculation. This factor, traceable to rotational invariance in the Minkowski space, causes the distribution to vanish at the maximum of $\not{E}$, which corresponds to zero three-momentum of the Z or the H. This is conducive to peaking behavior corresponding to each the two DM components, so long as the behavior of low $\not{E}$ is favored by angular momentum conservation, especially since there is now no collinear divergence at the higher end. One may thus see two peaks, the level of shift to the left for each peak being governed by the corresponding DM mass; their splitting thus becomes the deciding factor in the isolation of the peaks. An exceptional case is the operator O_1^f where the Z can be emitted via bremsstrahlung, for which the peak occurs at the higher end of $\not{E}$ spectrum for any DM mass due to the appearance of a small number $\sim m_Z^2/s$ in the denominator of the penultimate integrand. Feynman graphs that contribute to mono-V events ($V = \gamma, H, Z$) considered in this analysis are shown in Fig. 3, that are typical to result double bump in $\not{E}$ distributions.

We have used MadGraph [20] in tandem with DELPHES with the ILD card [21], as a result of which the behavior seen in the distributions deviate a little bit from the usual

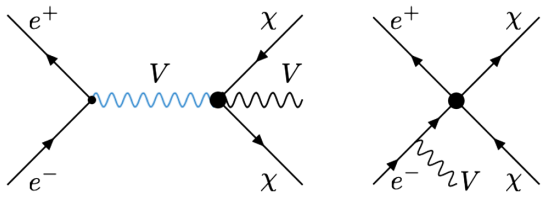


FIG. 3. Feynman graphs contributing to mono-V ($V = \gamma, H, Z$) events in this analysis.

ones. Specific beam polarization ($P_{e^+} = +30\%, P_{e^-} = +80\%$) choices are made to optimize the relative heights of both the peaks.

We also note that with appropriate combination of c, Λ, and $m_{\rm DM}$, it is possible to achieve the observed relic density from two DM-components constituted of the EFT operators in Table I, while addressing collider distinguishability, see the Supplemental Material [19].

Challenge 2: How to make the double peaks rise above the backgrounds? We have seen above some examples of cases where two peaks/bumps corresponding to the two DM particles are noticeable. However, it is not obvious that the peaks are distinct when different kinds of $\nu\bar{\nu}X(X = \gamma, Z, H)$ backgrounds as already shown in Figs. 1 and 2, are taken into account. At e^+e^- collider with $\sqrt{s} = 1$ TeV and polarizations $P_{e^+} = +30\%$ and $P_{e^-} = +80\%$, the corresponding SM backgrounds are as follows: 674.0 fb for $\nu\nu\gamma$, 46.6 fb for $\nu\nu H(b\bar{b})$, and 18.0 fb for $\nu\nu Z(\ell^+\ell^-)$.

While we consider all possible backgrounds, the most menacing ones that tend to drown the mono-Z and mono-H signals is the one from vector boson fusion (VBF). There are, after all, not too many kinematic variables at our disposal in this case. How then can one rise above the irreducible backgrounds?

Two generic criteria for this to happen, securing the best signal-to background ratio, are: (i) the signal peak that is closest to the SM background peak should rise as much above the latter as possible, and (ii) the other signal peak, after any distortion by the background, should still be as distinct from the first one as is possible.

In order to make the double peak distinct in spite of backgrounds, we propose a new observable here. This is the bin-by-bin signal significance $S/\sqrt{B}$ for an integrated luminosity ($\mathcal{L}$) optimized for different DM benchmarks. This "local significance," plotted against $\not{E}$, is shown in Figs. 4 (for mono-γ and mono-H) and 5 (for mono-Z). We present alongside the Gaussian fits of the corresponding histograms after minimizing χ^2, using:

$$G(t) = G_1(t) + G_2(t) + \mathcal{B} = A_1 e^{-\frac{(t-\mu_1)^2}{2\sigma_1^2}} + A_2 e^{-\frac{(t-\mu_2)^2}{2\sigma_2^2}} + \mathcal{B}. \quad (1)$$

The values of μ_1, μ_2, σ_1, and σ_2 in each case are indicated in the figure insets. In the examples shown here, we have

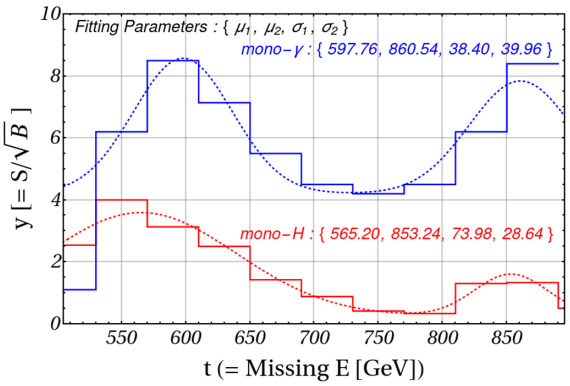


FIG. 4. Variation of local signal significance and Gaussian fitting as a function of $\not{E}$ for mono-γ signal (blue lines) with $\mathcal{L} = 100$ fb^{-1} as in Fig. 1 (top). The same are plotted for mono-H signal (red lines) as in Fig. 2 (top) at $\mathcal{L} = 1000$ fb^{-1}. Global signal significances = 5σ and $S/B \approx 4\%$ for mono-γ. For mono-H: 4.2σ and $S/B \approx 4\%$. Interestingly, in this case the signal-only distribution does not show a discernible double-peak behavior, but the bin-wise significance does, as shown here.

taken the bin size along the $\not{E}$-axis to be 40 GeV, which in most of cases optimize the significance. The central outcome of this is a rather remarkable distinctiveness of the two DM peaks, as evinced from the two Figs. 4 and 5. The global significance and the overall S/B are given in the corresponding figure captions; one can notice S/B ratios ranging up to 10%, and the global significance ranging between 4–5σ. This not only assures one of the usefulness of the suggested distributions but also indicates the level of refinement required in an e^+e^- experiment in connection with the reduction of systematic errors.

Is there any way of further improving the discernibility of the two peaks? In response to this query, we suggest

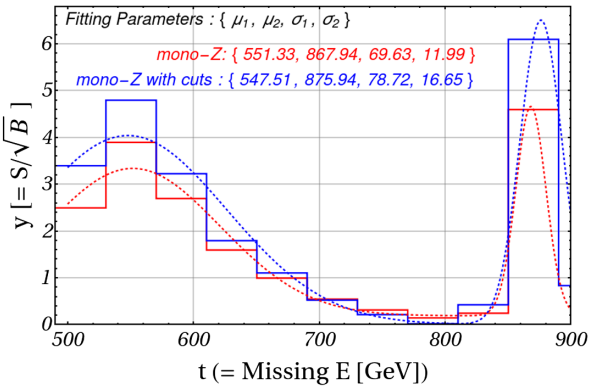


FIG. 5. Variation of local signal significance and Gaussian fitting as a function of $\not{E}$ for mono-Z signal (red lines) as in Fig. 2 (bottom) at $\mathcal{L} = 1000$ fb^{-1}. The same are plotted for the mono-Z signal after applying the cut $\not{E}_T < 50$ GeV or > 200 GeV at $\mathcal{L} = 1000$ fb^{-1} (blue lines). Global signal significance 4.7σ and $S/B \approx 5\%$ (red line). After applying the cuts, S/B increased to approximately 16%, and the global significance reached 7σ.

TABLE II. The combination of effective operators, signal significance and corresponding values of R_{C3} and R_{C4} for the chosen benchmarks, as discussed in Figs. 4 and 5. $\sigma_{\mathrm{DM}(1,2)}$ denote the individual contribution to the total cross section.

Benchmarks in	Operators	$\{m_{\mathrm{DM1}}, m_{\mathrm{DM2}}\}$ (GeV)	$\{\sigma_{\mathrm{DM1}}, \sigma_{\mathrm{DM2}}\}$ (fb)	$\mathcal{L}(\mathrm{fb}^{-1})$	S/B (%)	$S/\sqrt{B}$ (Global)	R_{C3}	R_{C4}
Figure 4 (mono-γ)	O_3^f, O_2^f	$\{100, 200\}$	$\{2.9, 9.9\}$	100	4	5.0σ	4	1.8
Figure 4 (mono-H)	O_2^s, O_1^s	$\{100, 400\}$	$\{0.4, 0.23\}$	3000	4	4.2σ	38	2.1
Figure 5 (mono-Z)	O_3^s, O_1^f	$\{100, 400\}$	$\{0.37, 0.42\}$	1000	5	4.7σ	16	7.1
Figure 5 (with cuts)	O_3^s, O_1^f	$\{100, 400\}$	$\{0.37, 0.42\}$	1000	16	7.0σ	23	23.8

further application of an $\not{E}_T$-cut on the signal and the backgrounds. Since $\not{E}_T$ and $\not{E}$ are *correlated only partially*, and the m_{DM} enters only into $\not{E}$ manifestly, one can, with judicious $\not{E}_T$ cuts, make the two peaks more distinct, and at the same time improve the global significance and the signal-to-background ratio. This is illustrated in Fig. 5 by the blue solid line. It should be remembered, though, that the $\not{E}_T$-cuts need to be customized after noticing the double-peak appearance first, lest one could either slice through the middle on a single peak and lead to fake double-peak events or reduce the height of one of the peaks in an actual double-peak event so that it effectively looks like a single peak.

The next question is: how to quantify the distinguishability of the two peaks in a mono-X signal? For this purpose we refer the reader to Ref. [22] where, in the context of the double-peak events generated in cascades, a number of distinction criteria $C_i (i = 1\text{–}4)$ have been developed; leading to the quantities $R_{C_i} (i = 1\text{–}4)$. The variables R_{C_3}, R_{C_4} emerge as the most useful ones, defined as,

$$R_{C3} = \frac{\int_{t_1}^{t_1^+} y dt - \int_{t_2^-}^{t_2^+} y dt}{\int_{t_1}^{t_1^+} y dt + \int_{t_2^-}^{t_2^+} y dt}, \quad R_{C4} = \frac{y(t') - y(t_{\min})}{\sqrt{y(t_{\min})}}, \tag{2}$$

where $y = G(t)$, $t_i^{\pm} = t_i \pm \Delta t$ with t_i denoting the mean value of ith peak of the two peak Gaussian function $G(t)$ and $t_{\min}$ denotes the local minima between the two peaks. In the definition of R_{C_4}, the parameter t' is specified as

$$t' = \begin{cases} t_2 & \text{if } y(t_2) < y(t_1), \\ t_1 & \text{if } y(t_2) > y(t_1). \end{cases}$$

R_{C3} reflects a comparative estimate of the number of events in the vicinity of the two peaks, and smaller R_{C3} implies that the second peak is more significant relative to the first one. R_{C4} quantifies the presence of the peaks with respect to the minimum in between, and its bigger values indicate better distinguishability. In Table II, we present the values corresponding to our chosen benchmark points, based on the Gaussian fits of the significance histograms. We note further that for the chosen benchmarks, (a) Mono-γ requires the least $\mathcal{L}$, (b) Mono-Z leads to the best distinguishability in terms of peak separation, and (c) Mono-H requires the maximum $\mathcal{L}$. The improvement brought about by the $\not{E}_T$ is also visible in Fig. 5. Similarly three peaks in the $\not{E}$ distribution from three DM's can be addressed by fitting a three-peak Gaussian distributions and subsequent analysis.

In Fig. 6, we explore the effect of m_{DM} in the distinguishability of the two peaks. We show the local $S/\sqrt{B} - \not{E}$ distribution for O_3^s (DM1) and O_2^f (DM2) for various choices of m_{DM}. It is clear that the distinguishability decreases with increasing m_{DM1} (see parameters R_{C_3}, R_{C_4} in the inset), resulting a decline in the global significance (also mentioned in the inset) due to smaller production cross-section. For some other examples, see the Supplemental Material [19].

In conclusion, mono-X events in an e^+e^- collider bring in a big challenge in distinguishing between two DM components. This is in contrast to DM signals produced in cascades, where not only are backgrounds are easier to reduce, but the occurrence of two peaks is also a more widespread phenomenon, as has been demonstrated in [22]. Our analysis of mono-X events identifies the physics underlying double-peak occurrence; we also demonstrate that bin-by-bin distributions in signal significance plotted against $\not{E}$ obviates the double-peaking behavior which the backgrounds otherwise tend to obliterate. It is also found by

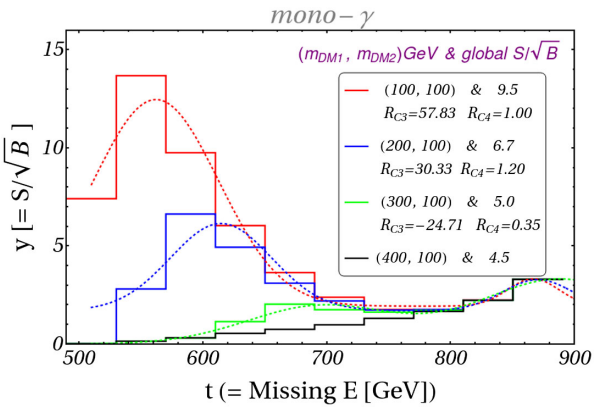


FIG. 6. Variation of local signal significance and Gaussian fitting as a function of $\not{E}$ for mono-γ signal for the operator set O_3^s (DM1) and O_2^f (DM2) with various combinations of m_{DM} at $\mathcal{L} = 3000\ \mathrm{fb}^{-1}$. R_{C_3}, R_{C_4} and global significance for each combination is mentioned in the inset.

us that judicious $\not{E}_T$ cuts serve to enhance the prominence of the two peaks as well as overall significance and signal-to-background ratios. We shall discuss in a more detailed paper other issues such as the demands on our sample theoretical scenario brought about by issues such as relic density or direct searches [23].

One point is worth emphasizing at the end. There may be occasions where the DM signal actually yields a single peak due to one DM component, but a fortuitous background pattern creates the semblance of a second peak. The bin-wise significance comes to the rescue, where one ends up with two-peak only at the presence of the two DM components provided they give rise to adequate signal rates individually and are made distinct through the variables discussed here.

S. B. acknowledges the Grant No. CRG/2019/004078 from SERB, Govt. of India. P. G. would like to acknowledge Indian Association for the Cultivation of Science, Kolkata for the financial support.

[1] Q.-H. Cao, E. Ma, J. Wudka, and C. P. Yuan, Multipartite dark matter, arXiv:0711.3881.
[2] S. Bhattacharya, A. Drozd, B. Grzadkowski, and J. Wudka, Two-component dark matter, J. High Energy Phys. 10 (2013) 158.
[3] J. Herrero-Garcia, A. Scaffidi, M. White, and A. G. Williams, On the direct detection of multi-component dark matter: Implications of the relic abundance, J. Cosmol. Astropart. Phys. 01 (2019) 008.
[4] M. Aoki and T. Toma, Boosted self-interacting dark matter in a multi-component dark matter model, J. Cosmol. Astropart. Phys. 10 (2018) 020.
[5] G. Belanger, A. Mjallal, and A. Pukhov, Two dark matter candidates: The case of inert doublet and singlet scalars, Phys. Rev. D **105**, 035018 (2022).
[6] J. Hernandez-Sanchez, V. Keus, S. Moretti, and D. Sokolowska, Complementary collider and astrophysical probes of multi-component dark matter, J. High Energy Phys. 03 (2023) 045.
[7] K. Fujii *et al.*, The role of positron polarization for the initial 250 GeV stage of the international linear collider, arXiv:1801.02840.
[8] M. Habermehl, M. Berggren, and J. List, WIMP dark matter at the international linear collider, Phys. Rev. D **101**, 075053 (2020).
[9] N. F. Bell, J. B. Dent, A. J. Galea, T. D. Jacques, L. M. Krauss, and T. J. Weiler, Searching for dark matter at the LHC with a Mono-Z, Phys. Rev. D **86**, 096011 (2012).
[10] A. Berlin, T. Lin, and L.-T. Wang, Mono-Higgs detection of dark matter at the LHC, J. High Energy Phys. 06 (2014) 078.
[11] E. Tolley (ATLAS Collaboration), Dark matter searches with Mono-X signatures at the ATLAS experiment, Proc. Sci. DIS2016 (**2016**) 107.
[12] A. M. Sirunyan *et al.* (CMS Collaboration), Search for new physics in the monophoton final state in proton-proton collisions at $\sqrt{s} = 13$ TeV, J. High Energy Phys. 10 (2017) 073.
[13] E. Bernreuther, J. Horak, T. Plehn, and A. Butter, Actual physics behind Mono-X, SciPost Phys. **5**, 034 (2018).
[14] S. Bottaro, D. Buttazzo, M. Costa, R. Franceschini, P. Panci, D. Redigolo, and L. Vittorio, Closing the window on WIMP dark matter, Eur. Phys. J. C **82**, 31 (2022).
[15] P. J. Fox, R. Harnik, J. Kopp, and Y. Tsai, LEP shines light on dark matter, Phys. Rev. D **84**, 014028 (2011).
[16] Y. J. Chae and M. Perelstein, Dark matter search at a linear collider: Effective operator approach, J. High Energy Phys. 05 (2013) 138.
[17] S. Kundu, A. Guha, P. K. Das, and P. S. B. Dev, A model-independent analysis of leptophilic dark matter at future electron-positron colliders in the mono-photon and Mono-Z channels, Phys. Rev. D **107**, 015003 (2023).
[18] B. Barman, S. Bhattacharya, S. Girmohanta, and S. Jahedi, Effective leptophilic WIMPs at the e^+e^- collider, J. High Energy Phys. 04 (2022) 146.
[19] See Supplemental Material at http://link.aps.org/supplemental/10.1103/PhysRevD.108.L111703 for exceptional cases, such as two DMs arising from the same operator, a single DM interacting via different operators, relic density constraints, and the effect of mass in distinguishing the DM components.
[20] J. Alwall, M. Herquet, F. Maltoni, O. Mattelaer, and T. Stelzer, MadGraph 5: Going beyond, J. High Energy Phys. 06 (2011) 128.
[21] J. de Favereau, C. Delaere, P. Demin, A. Giammanco, V. Lemaître, A. Mertens, and M. Selvaggi (DELPHES 3 Collaboration), DELPHES 3, A modular framework for fast simulation of a generic collider experiment, J. High Energy Phys. 02 (2014) 057.
[22] S. Bhattacharya, P. Ghosh, J. Lahiri, and B. Mukhopadhyaya, Distinguishing two dark matter component particles at e^+e^- colliders, J. High Energy Phys. 12 (2022) 049.
[23] S. Bhattacharya, P. Ghosh, J. Lahiri, and B. Mukhopadhyaya (to be published).